Journal of Alloys and Compounds 505 (2010) 698–711

Contents lists available at ScienceDirect

Journal of Alloys and Compounds

journal homepage: www.elsevier.com/locate/jallcom

Structural, electronic and optical properties of ZnX and CdX compounds (X = Se, Te and S) under hydrostatic pressure

Z. Nourbakhsh*

Physics Department, Faculty of Science, University of Isfahan, Isfahan, Iran

ARTICLE INFO

Article history:
Received 11 October 2009
Received in revised form 12 June 2010
Accepted 14 June 2010
Available online 30 June 2010

PACS:
74.25.Gz
71.15.Mb
74.25.Jb

Keywords:
Semiconductors
Electronic band structure
Optical properties
Dielectric function

ABSTRACT

The structural, electronic and optical properties of ZnX and CdX (X = Se, Te and S) are studied using density functional theory by the Wien2k package. The energy band gap, real and imaginary parts of the dielectric function, energy loss function, optical absorption coefficient and reflectivity spectra of these compounds are calculated. The Engel–Vosko approach improves the energy band gaps of ZnX and CdX compounds. The calculated optical parameters are in good agreement with available experimental results, particularly in the Engel–Vosko approach. Furthermore the effect of hydrostatic pressure on the energy band gap, the real and imaginary parts of the dielectric function of these compounds is studied. The first and second order pressure coefficient for the energy band gaps, the static dielectric function and the static reflectivity spectra are calculated.

1. Introduction

ZnX compounds have cubic (zinc blende) structure [1–3], whereas CdX compounds depending on the growth condition may have both zinc blende and wurtzite (hexagonal) structures at normal conditions. Theoretical studies indicate that CdX compounds are stable in both zinc blende and wurtzite structures [2,4–8], while experimental observations show that CdS and CdSe are stable in wurtzite structure and CdTe in zinc blende [9–12]. These compounds have attracted much attention, because they have direct energy band gaps and are light emitters at normal conditions [1,2,13–16]. Moreover they appear to be promising candidates for many technological applications [17], such as blue laser fabrication techniques, optoelectronic devices operating in the visible light range and in UV photodetectors and modulated hetero structures, light emitting diode, reflector, dielectric filter, optical switching devices, optical wave guides, high density optical memories, solar cells, photovoltaic cells [18], etc. There have been considerable applications in the area of nanostructures, such as nano-wires, thin films, quantum dot lasers as well as those related to passivating the surface of other materials to create confined particles [19–21], etc. There have been many empirical and ab initio calculations of the electronic and optical properties for these compounds [22–32]. Reshak and Auluck [32] analyzed the electronic and optical properties of ZnX compounds within local density approximation (LDA) and generalized gradient approximation (GGA). Sapra et al. [22] used the linear muffin-tin orbital approach to calculate the band structure of ZnX compounds and Karazhanov et al. [33] used the density functional theory to calculate the electronic, structural and optical properties of ZnX compounds. Bang et al. [34] used spectroscopic ellipsometry to measure the real and imaginary parts of the dielectric function of ZnX compounds. Freeouf [35] used synchrotron radiation and standard light source to measure the polarization dependent optical properties of ZnX compounds. Ronnow et al. [36] measured the piezo-optical coefficients of ZnSe and ZnTe using reflectance difference spectroscopy. He et al. [10] and Sowa [9] studied the phase transition of CdS and CdSe compounds respectively. Reddy et al. [23] investigated the interrelationship between the structural, optical, electronic and elastic properties of ZnX and CdX compounds. Khenata et al. [37] used the full potential linearized augmented plane wave plus local orbital method to calculate the elastic, electronic and optical properties of ZnS, ZnSe and ZnTe under pressure. Deligoz et al. [38] investigated the electronic and lattice dynamical properties of CdS, CdSe and CdTe. Kirin and Lukačević [39] studied the stability of high pressure phases of ZnS, ZnSe, CdS and CsSe compounds. Hosseini [6] calculated the dielectric functions of CdTe. Merad et al. [40] studied the electronic and optical properties of CdTe and ZnTe.

* Tel.: +98 311 7932425; fax: +98 311 7932409.
E-mail address: z.nourbakhsh@phys.ui.ac.ir.

0925-8388/$ – see front matter © 2010 Elsevier B.V. All rights reserved.
doi:10.1016/j.jallcom.2010.06.120

The first goal of this paper is to compare and investigate the structural, electronic and optical properties of ZnX and CdX (X = S, Se and Te) compounds within LDA [41], GGA [42] and Engel–Vosko generalized gradient approximation (GGA_EV) [43] at zero pressure. Since the structural, electronic and optical properties of these compounds at zero pressure have already been reported by others, the author has compared the results with previous calculations and experimental data and has focused on those features of the electronic and optical properties that have not been touched by others. In other words, to complete the existing theoretical works on these compounds, the author has compared the degree of covalency and ionicity, the peaks location of real and imaginary parts of dielectric function of ZnX with CdX compounds. The author has focused on the conduction and valence bandwidth, the mobility of electrons and holes, the static dielectric function and the static reflectivity of these compounds using LDA, GGA and GGA_EV. The second goal of this paper is to investigate the effect of pressure on the electronic and optical properties of these compounds within LDA, GGA and GGA_EV. The theoretical studies carried out on the electronic and optical properties of these compounds under pressure are limited. The author has focused on the effect of pressure on the valence and conduction bandwidth, static dielectric function and the static reflectivity spectra of these compounds. In addition, the author revised the results on the pressure dependence of the static dielectric function of ZnS, ZnSe and ZnTe compounds reported by Khenata et al. [37].

The paper is organized as follows: In Section 2, a brief description of the method used and details of the calculations are given. In Section 3, the results of structural, electronic and optical properties are presented and analyzed. Conclusions are drawn in the last section.

2. Method of calculations

Density functional theory (DFT) is the most widely used first-principles method for the calculation of the structural, electronic and optical properties of solids. The calculated results in this paper were obtained using the full potential linearized augmented plane wave plus local orbital (APW + lo) method as implemented in the Wien2k code [44]. The approach is based on the DFT within the LDA, using the scheme of Ceperley–Alder as parameterized by Perdew–Zunger [41], GGA96 [42] using the scheme of Perdew–Burke–Ernzerhof and GGA_EV [43]. The GGA_EV has been developed for calculation of the energy band structure, which is based on potential optimized but not for computations of structural parameters. In the APW method, each unit cell is divided into non-overlapping muffin-tin (MT) spheres of radii R_{MT} and an interstitial region, where the Kohn–Sham wave functions are expressed in spherical harmonics within the MT spheres and in plane waves in the interstitial region. The charge density and the crystal potential are expanded in spherical harmonics inside muffin-tin spheres, and in plane waves in the interstitial region. The parameters used in this calculation were chosen as follows:

The radii of the muffin-tin spheres were chosen as $R_{Zn,Cd} = 1.9$ a.u. and $R_X = 1.8$ a.u. To provide a reliable Brillouin zone integration, a set of 204 k-points in the irreducible wedge of the Brillouin zone was used for self-consistency while a finer mash of 440 k-points (in the irreducible wedge of the Brillouin zone)

Table 1
The calculated lattice constants (Å) of ZnX and CdX compounds.

	Compounds		LDA	GGA	Expt.	Other works
Zinc blende	ZnS		5.29	5.44	5.41[a]	5.45[b]
	ZnSe		5.57	5.73	5.67[c]	5.747[d]
	ZnTe		6.07	6.16	6.1[c]	6.195[d]
	CdS		5.75	5.93	5.82[b]	5.87[b]
	CdSe		6.00	6.19	6.05[e]	6.084[f]
	CdTe		6.38	6.61	6.48[c]	6.48[f]
Wurtzite	ZnS	a	3.74	3.84	3.816[a]	3.89[b]
		c	6.12	6.29	6.252[a]	6.20[b]
		u	0.3721	0.3733		0.374[g]
	ZnSe	a	3.66	3.77	3.99[f]	3.99[h]
		c	6.08	6.26	6.62[f]	6.62[h]
		u	0.3718	0.3729		0.371[i]
	ZnT	a	4.38	4.45	4.32[f]	4.366[j]
		e	7.03	7.21	7.100[f]	7.176[j]
		u	0.3716	0.3727		0.373[j]
	CdS	a	4.07	4.19	4.14[c]	4.19[b]
		c	6.60	6.80	6.7[c]	6.66[b]
		u	0.3738	0.3759	0.37715[k]	0.3757[l]
	CdSe	a	4.04	4.51	4.3[c]	4.29[m]
		c	6.60	7.36	7.01[c]	7.01[m]
		u	0.3742	0.3758	0.3759[m]	0.3756[l]
	CdTe	a	4.53	4.61		4.5499[l]
		c	7.41	7.53		7.4512[l]
		u	0.3748	0.3755		0.3754[l]

[a] Ref. [49].
[b] Ref. [2].
[c] Ref. [29].
[d] Ref. [52].
[e] Ref. [55].
[f] Ref. [14].
[g] Ref. [40].
[h] Ref. [54].
[i] Ref. [45].
[j] Ref. [46].
[k] Ref. [47].
[l] Ref. [48].
[m] Ref. [50].

was employed for the calculation of the optical properties. All the calculations were highly converged with respect to k-points. The angular momentum quantum number as a cutoff for expanding the Kohn–Sham wave functions in terms of lattice harmonics inside the muffin-tin sphere was confined to $l_{max} = 10$. The wave function cutoff for the plane wave expansion of the wave function in the interstitial region was $K_{max} = 8/R_{MT}\,(\text{a.u.})^{-1}$ where R_{MT} is the smallest muffin-tin radius in the unit cell. The charge density and the potential were Fourier expanded in the interstitial region up to $G_{max} = 14\,(\text{Ry})^{1/2}$.

3. Results and discussion

3.1. Structural properties

In order to calculate the ground state properties of ZnX and CdX (with X = Se, Te and S) compounds, the total energy as a function of the unit cell volume is calculated in the zinc blende and wurtzite structures using GGA, LDA and GGA_EV. For the geometric equilibrium determination of the wurtzite phase the author proceeded as follows: The internal parameters for each volume have been optimized by relaxing the atomic positions in the force direction. Then the optimized internal parameters are used to optimize the c/a ratio. Using the optimized c/a ratio, once again more accurate values of the internal parameter are calculated. The calculated internal parameters within LDA and GGA are given in Table 1. The calculated internal parameters are in good agreement with available experimental and other theoretical works [4,40,45–47]. In zinc blende and wurtzite structures, the calculated total energy for several volumes is fitted with the Murnaghan equation of state [48]. Due to the close similarity between the total energy–volume behaviors of ZnX and CdX compounds, the total energy–volume curves within LDA, GGA and GGA_EV in the zinc blende and wurtzite structures are given only for the CdSe compound in Fig. 1. The calculated energy volume curves within GGA_EV indicate that this approximation does not well produce total energy. At zero pressure, the most stable phases are the wurtzite according to GGA and the zinc blende according to LDA. The energy differences between the zinc blende and wurtzite phases are extremely small, of the order of meV. Thus, these compounds can take both cubic as well as hexagonal structure. The corresponding equilibrium lattice constants and bulk moduli of ZnX and CdX compounds in zinc blende and wurtzite phases, as calculated within LDA and GGA, are compared with experimental values and other works in Tables 1 and 2. The calculated equilibrium lattice constants and bulk moduli obtained in LDA and GGA are in good agreement with the experiment.

The author expects the unit cell volumes of ZnX and CdX compounds to be related to the size of the component atoms with some adjustment for bonding in the solid. Such a bonding contribution should be approximately constant for a given column in the periodic table for which the number of valence electrons is constant. Thus the lattice constants of, for example, ZnS, ZnSe and ZnTe should be proportional to the size of the S, Se and Te atoms, and the lattice constant should increase down a column of the periodic table. The calculated lattice constants of ZnX and CdX compounds show that, the lattice constants of CdX are larger than those of ZnX and increase when S is replaced by Se and Se by Te in cubic and hexagonal phases.

Al-Douri et al. have shown that the dominant effect on the bulk moduli of semiconductors is from the degree of covalency and ionicity [57–59]. The bulk modulus generally increases with increasing covalency. The effect of ionicity is to reduce the amount of bonding charge and hence to reduce the bulk modulus. ZnX and CdX compounds are characterized by different degrees of covalent and ionic

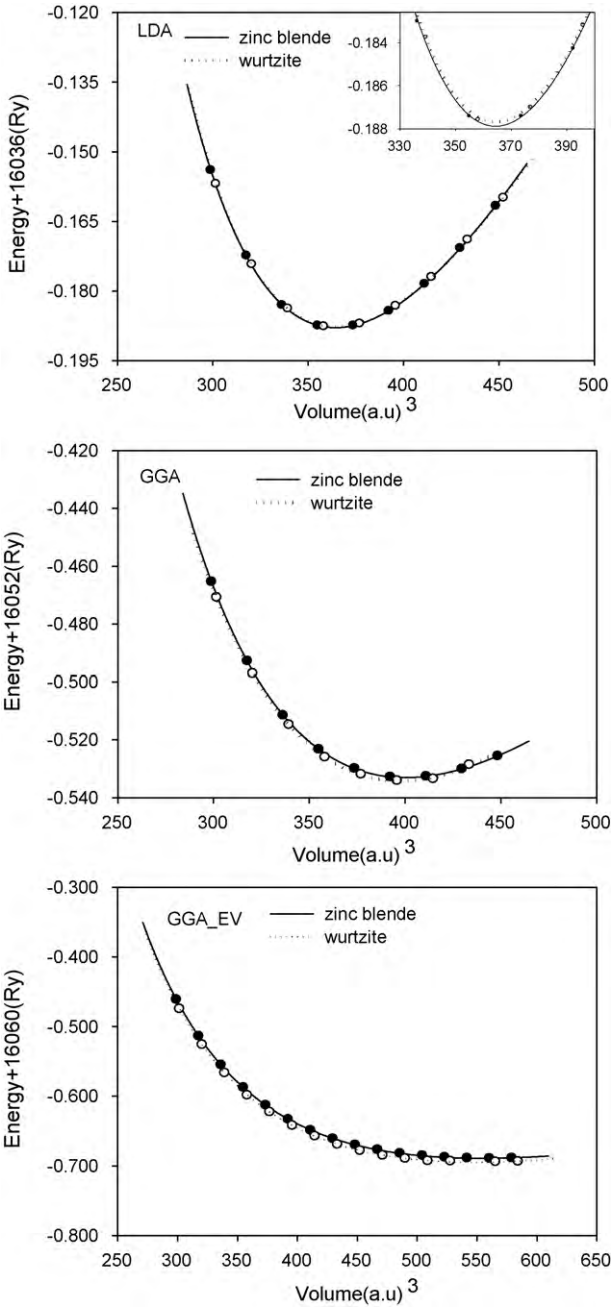

Fig. 1. The total energy–volume curves of CdSe within LDA, GGA and GGA-EV in the zinc blende and wurtzite structures.

bonding. The calculated bulk modulus of these compounds in cubic and hexagonal phases show that,

(i) Going along a row from ZnX to CdX compounds, the bulk modulus decreases. This is due to the increase of ionicity and loss of covalency (as will be shown in Section 3.2.1).
(ii) The bulk modulus of ZnX and CdX compounds decreases as the atomic number of X atom increases. This trend is due to covalency decreasing with increasing nearest neighbor distance.

3.2. Electronic properties

3.2.1. Band structure and density of states

To investigate the electronic properties of ZnX and CdX compounds, the author has calculated the band structure and electron

Table 2
The bulk modulus (GPa) of ZnX and CdX compounds.

	Compounds	LDA	GGA	Expt.	Other works
Zinc blende phase	ZnS	85.70	68.22	76.9[a]	75.6[b] 85.2[c]
	ZnSe	70.93	56.55	62.5[a]	69[d] 56.8[e]
	ZnTe	43.95	43.84	51[f,a] 50.9[g]	43.6[e] 65.1[c]
	CdS	67.43	52.60	62[g]	65.5[b] 72.42[h]
	CdSe	57.81	45.94	53[g]	65.2[h]
	CdTe	46.22	34.00	42[f]	48.94[h]
Wurtzite phase	ZnS	85.82	68.00	74.0[b]	76.4[b]
	ZnSe	70.59	55.84		
	ZnTe	50.37	46.24		55.3[i]
	CdS	67.19	52.89	61.5[a]	62.8[b]
	CdSe	57.58	44.78	55[a]	57.9[j]
	CdTe	44.31	37.23	42.1[a]	46.2[i]

[a] Ref. [29].
[b] Ref. [2].
[c] Ref. [53].
[d] Ref. [51].
[e] Ref. [52].
[f] Ref. [56].
[g] Ref. [55].
[h] Ref. [38].
[i] Ref. [37].
[j] Ref. [4].

density of states in the cubic and hexagonal structures within LDA and GGA, using calculated equilibrium lattice constants as obtained in Section 3.1. The results of this calculation show that the general features of the band structures of ZnX and CdX compounds are similar, with small differences in bandwidths. The valence bandwidth of ZnX is larger than that of CdX. This effect arises from the hybridization accompanying the change in bonding from more ionic to more covalent, as Zn is replaced by Cd. In all cases, the valence band maximum and the conduction band minimum occur at the Γ point, hence these compounds are semiconductors with direct energy band gaps. For the same X atom, this direct energy band gap decreases from Zn to Cd. Furthermore using the calculated band structure the author has calculated the energy band gaps of these compounds within LDA and GGA. The results of this calculation are compared with experimental values and results from other works in Table 3, this comparison shows that the calculated band gaps within LDA and GGA are smaller than experimental values. It is well known that in self-consistent band structure calculation using DFT, both LDA and GGA usually underestimate the energy band gap. Engel and Vosko [43] constructed a new functional form of GGA (GGA_EV) to calculate the exchange correlation potential which optimizes exchange potential (V_x) for band structure calculations. Since GGA-EV was developed to yield a better V_x, the author now wants to demonstrate that it really improves the results, such as the band structure which mainly depends on the accuracy of V_x [43]. Dufek and Blaha [60] applied GGA_EV to a wide range of solids and compared the results with other GGA calculations. They concluded that the GGA_EV improves the determination of the band gap and some other properties. The author has calculated the band structure and electron density of states of these compounds within GGA_EV using the calculated equilibrium lattice constants within GGA (as obtained in Section 3.1). The calculated band structures within GGA_EV are similar to LDA and GGA: the only differences are in band splitting value. Due to the close similarity between band structures within the LDA, GGA and GGA_EV, in this part the band structure is given only in the cubic phase within the GGA_EV.

Table 3
The calculated energy band gap (eV) of ZnX and CdX compounds within LDA, GGA and GGA-EV.

Compound	Zinc blende			Wurtzite			Expt.	Other works
	LDA	GGA	GGA-EV	LDA	GGA	GGA-EV		
ZnS	1.85	2.1	3.27	1.89	2.12	2.8	3.68[a]	3.34[b] 2.16[c]
ZnSe	1.07	1.29	2.2	1.05	1.3	2.3	2.7[a]	1.86[d] 1.65[b]
ZnTe	1.05	1.23	1.78	1.02	1.27	1.83	2.26[a]	1.58[d] 2.27[b]
CdS	0.9	1.15	1.92	0.95	1.2	2.05	2.485[a]	2.15[b] 1.45[e]
CdSe	0.36	0.71	1.35	0.41	0.72	1.37	1.75[a]	1.48[b] 1.08[e]
CdTe	0.5	0.61	1.33	0.38	0.63	1.34	1.43[a]	1.24[b] 1.88[e]

[a] Ref. [29].
[b] Ref. [23].
[c] Ref. [37].
[d] Ref. [52].
[e] Ref. [38].

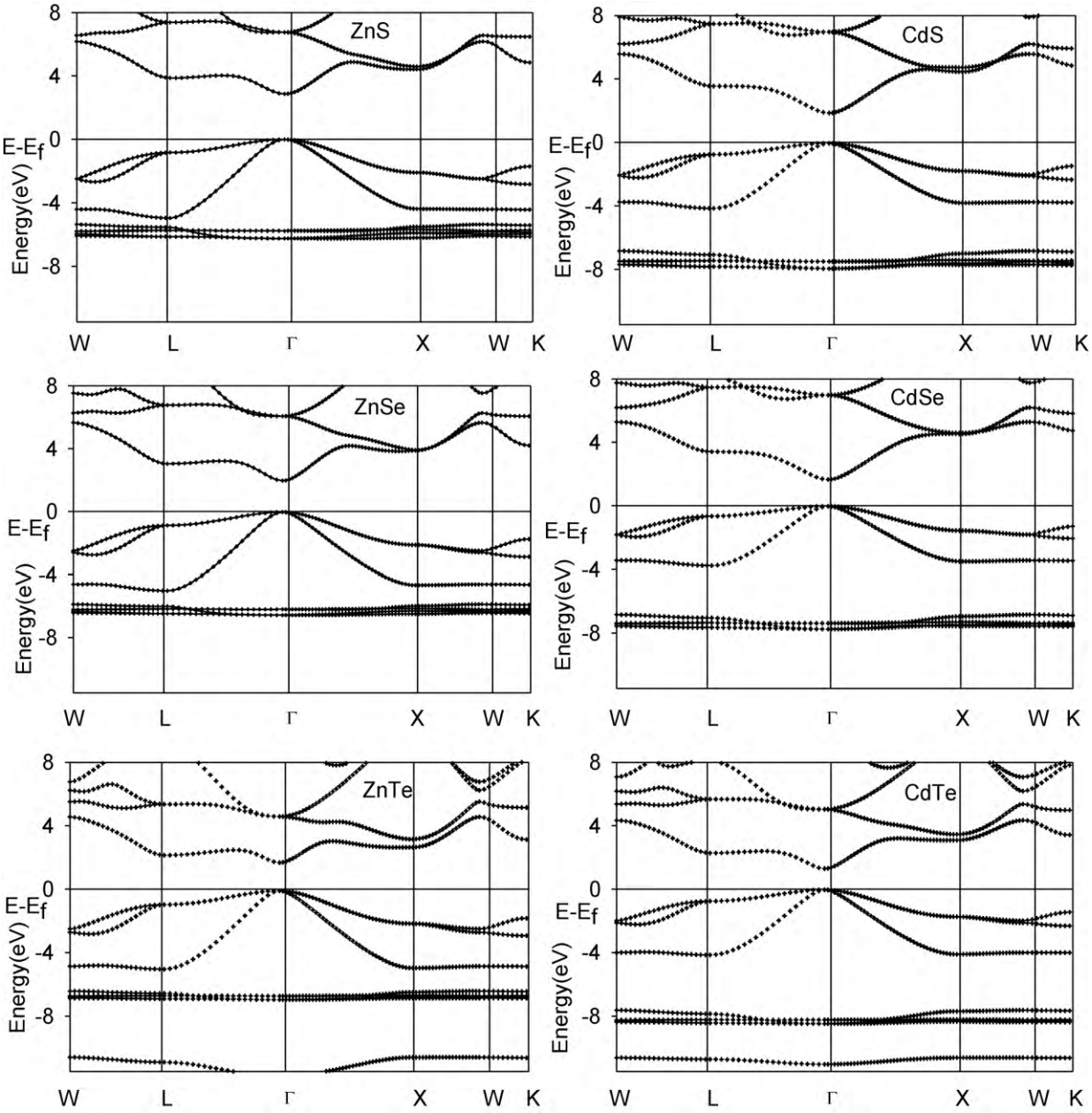

Fig. 2. The band structure of ZnX and CdX compounds in GGA_EV using the equilibrium lattice constant according to GGA in zinc blende phase.

Results are shown in Fig. 2. It is seen that the conduction bands are more dispersive than the valence bands. The reason lies in the fact that they are more delocalized. The general features of the band dispersions are in agreement with previous studies [52]. The conduction band minima are much more dispersive than the valence band maxima, which show that the holes are much heavier than the conduction band electrons. Consequently, the mobility of the electrons is higher than that of the holes. Furthermore, these features indicate that the p electrons of X atom (topmost valence band states) are tightly bound to their atoms and make the valence band holes less mobile. Hence, the contribution of the holes to the conductivity is expected to be smaller than that of conduction band electrons even though the concentration of the latter is smaller than that of the former. These features emphasize the predominant ionic nature of the chemical bonding. Another interesting feature of the band structures is that the valence band maximum becomes more dispersive with increase in the atomic number of X atom.

The calculated energy band gaps of ZnX and CdX compounds in wurtzite and zinc blende phases within GGA_EV are also given in Table 3. The calculated energy band gaps in wurtzite phases are very close to the corresponding values for the zinc blende phases. The results show that the value of the band gap within GGA_EV is improved considerably. In some previous papers [60], it has been suggested that for some semiconductors, the calculated energy band gap with GGA-EV is closer to the experimental value than the one obtained with LDA and GGA. Comparing the calculated energy band gaps and experimental values shows that for the same X atom the energy band gap of ZnX is larger than CdX and the energy band gap of ZnX and CdX compounds decrease as the atomic number of X atom increases. The author notes that this trend in energy gap is in agreement with experimental data.

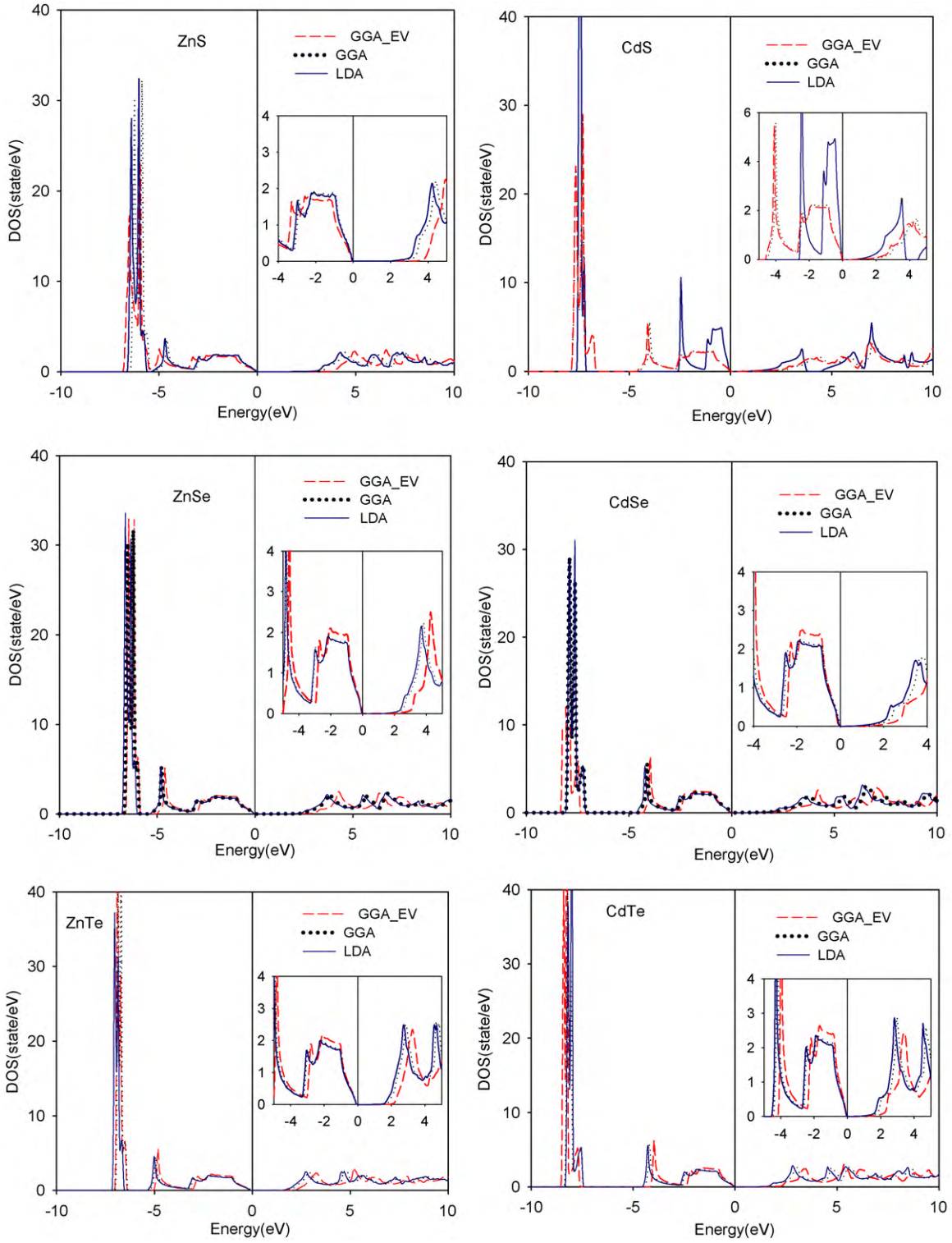

Fig. 3. The total electron density of states for ZnX and CdX compounds within LDA, GGA and GGA_EV.

Furthermore the calculated total electron density of states (DOS) of ZnX and CdX compounds within LDA, GGA and GGA-EV are shown in Fig. 3. The electron density of state is similar for all compounds, with some small differences in details. The major contribution to the occupied part of the electron density of states around the Fermi energy comes from the p states of the X atom and the s states of Zn and Cd. The low-lying energy side of DOS consists of a narrow peak centered on −7 eV for ZnX compounds and at −8 eV for CdX. This peak shifts toward higher energy level when Te is replaced by Se and further by S. This peak originates from the d orbital of Zn and Cd atoms, and is highest for X = Te and lowest for X = S. The electron density of states above the Fermi energy originates mainly from the s and p states of Zn or Cd, partially mixed with some d states. The above mentioned electron density of states within the GGA_EV are pushed toward the outer layer, this is the reason for the energy gap improvement.

Table 4
The transition pressures (GPa) of ZnX and CdX from zinc blende phases to rocksalt phase, experimental values and other works. The transition pressures of ZnTe and CeTe from zinc blend phase to cinnabar phase are given in parenthesis.

	ZnS	ZnSe	ZnTe	CdS	CdSe	CdTe
This work	16.4	14.3	15.2 (12.2)	5.5	5.2	4.3 (3.5)
Expt.	14.7[a,b]	13–15[a]	8.9–9.5[a]	2.3–2.7[a]	2.5[a]	3.53[a]
Other work	15.5[c], 11.4[d] 17.5[i]	13.5[c] 15.2[j]		2.7[e], 3.1[f]	2.5[g]	3.31[h]

[a] Ref. [72].
[b] Ref. [43].
[c] Ref. [62].
[d] Ref. [74].
[e] Ref. [67].
[f] Ref. [68].
[g] Ref. [10].
[h] Ref. [12].
[i] Ref. [62].
[j] Ref. [71].

3.2.2. Pressure dependence of the energy band gap

An understanding of the high pressure phase transformations of ZnX and CdX compounds has long been impeded by uncertainties. ZnX and CdX compounds indicate four phases: zinc blende, rocksalt, cinnabar and the simple cubic SC16 structure at different pressures. In addition, the body centered tetragonal ($\beta-$Sn) structure for ZnS and the two different orthorhombic structures have been reported for CdTe. Theoretical calculations [61,62] have been shown that ZnS has two intermediate high pressure phases, SC16 and the cinnabar below the pressure range of the rocksalt structure. The SC16 and cinnabar structures for ZnS have not been observed experimentally. ZnS undergoes a high pressure phase transition from rocksalt into the body centered tetragonal ($\beta-$Sn) structure. Theoretical calculations for ZnSe indicate that SC16 is stable in the pressure range of 9.2–16.4 GPa and the cinnabar structure is unstable as a high pressure phase [63]. Kusaba and Kikegawa [64] reported the existence of ZnSe in the cinnabar structure in the pressure region of 9–11 GPa. There is no experimental evidence for the existence of ZnSe in SC16 structure. A combined extended X-ray absorption fine structure and energy dispersive X-ray diffraction study proposed the cinnabar structure for ZnTe [65]. The SC16 structure was observed above the stability pressure range of the cinnabar structure. The cinnabar is more stable than the SC16 structure [66]. The presence of the rocksalt structure for ZnTe remains unclear. Experimental and theoretical studies have shown that CdSe and CdS compounds have a phase transition from zinc blende or wurtzite into rocksalt structure under hydrostatic pressure [10,67,68], while the phase transition of CdTe compound is from zinc blende to cinnabar then to rocksalt structure [12,69]. CdTe undergoes a continuous phase transition from rocksalt to orthorhombic (Cmcm) structure at 10 GPa. A further transition of CdTe, to an orthorhombic structure with space group Pmm2, has been reported at 12 GPa [68,69]. The author has studied the phase transition of ZnX and CdX compounds. The pressure for the phase transition from zinc blende to rocksalt structure is determined by the common tangent of the two energy–volume curves. The slope of this tangent gives the calculated transition pressure, which is defined as the pressure where the enthalpies of both structures are equal. The author has calculated the pressure transition of ZnX and CdX compounds from the zinc blende to the rocksalt structure and ZnTe and CdTe compounds from zinc blend to cinnabar structure. The calculated results are given in Table 4, together with available theoretical and experimental data [10,12,62,67–74]. The calculated phase transition pressure of ZnX is in agreement with experimental values, while for CdX it is higher than the experimental values.

To investigate the effect of pressure on the band structure of ZnX and CdX compounds, the author has calculated the band structure of these compounds within GGA_EV at different pressures. The pressure was calculated within GGA and applied to calculate the band structure within GGA_EV. The band structure calculation of these compounds indicates that ZnX and CdX compounds have direct band gap over the whole pressure range considered ($p \leq 20$ GPa). The author has calculated the energy band gap, valence bandwidth and conduction bandwidth at different pressures. The results are shown in Fig. 4. They show that the valence bandwidth increases with increasing pressure, while pressure does not have any considerable effect on the conduction bandwidth of these compounds. In general, the valence bandwidth becomes larger as a semiconductor becomes less ionic. This reflects the decreases of the ionic character of these compounds under pressure. It should be noted that the maximum of the valence band at Γ point shifts downward under pressure while the conduction band minimum at Γ point goes up. Consequently the direct band gap at the Γ point increases under pressure. In the case of the above mentioned investigated compounds the variation of direct band gap with pressure is not linear. The calculated results are fitted to a second order polynomial:

$$E_g(p) = E_g^0 + \alpha p + \beta p^2$$

where E_g^0 (eV) is the energy gap at zero pressure, p (GPa) is the pressure, α and β are the first and second order pressure coefficients respectively. The calculated results, experimental values and other works are given in Table 5. The calculated first and second order pressure coefficients of ZnX compounds are in better agreement with experiment compared to other theoretical work which is based on LDA. To my knowledge, there are no experimental nor theoretical values of the second order pressure coefficients for CdX compounds to compare with. The author leaves these results as references for future investigation. The first order pressure coefficients of an interband transition n depends on the volume deformation potential $dE_n/d\ln(V)$ and bulk modulus (B) via the relation $\alpha^n = (-1/B)(dE_n/d\ln(V))$. The first order pressure coefficients of ZnX and CdX compounds increase with increasing X atomic number. This increase in the linear pressure coefficient is mainly due to the decrease in bulk modulus when X atomic number increases. The first order pressure coefficients of ZnX compounds are larger compared to corresponding ones in CdX, while the bulk modulus of ZnX compounds is larger than CdX compounds. For a system containing an active d orbital (e.g. ZnX and CdX), the increase of the first order coefficients induced by the reduction of the bulk modulus is partially canceled by the d–p repulsion. The smaller value of the first order pressure coefficients of CdX compounds is due to the strong p–d coupling in CdX compare to ZnX which shifts up the

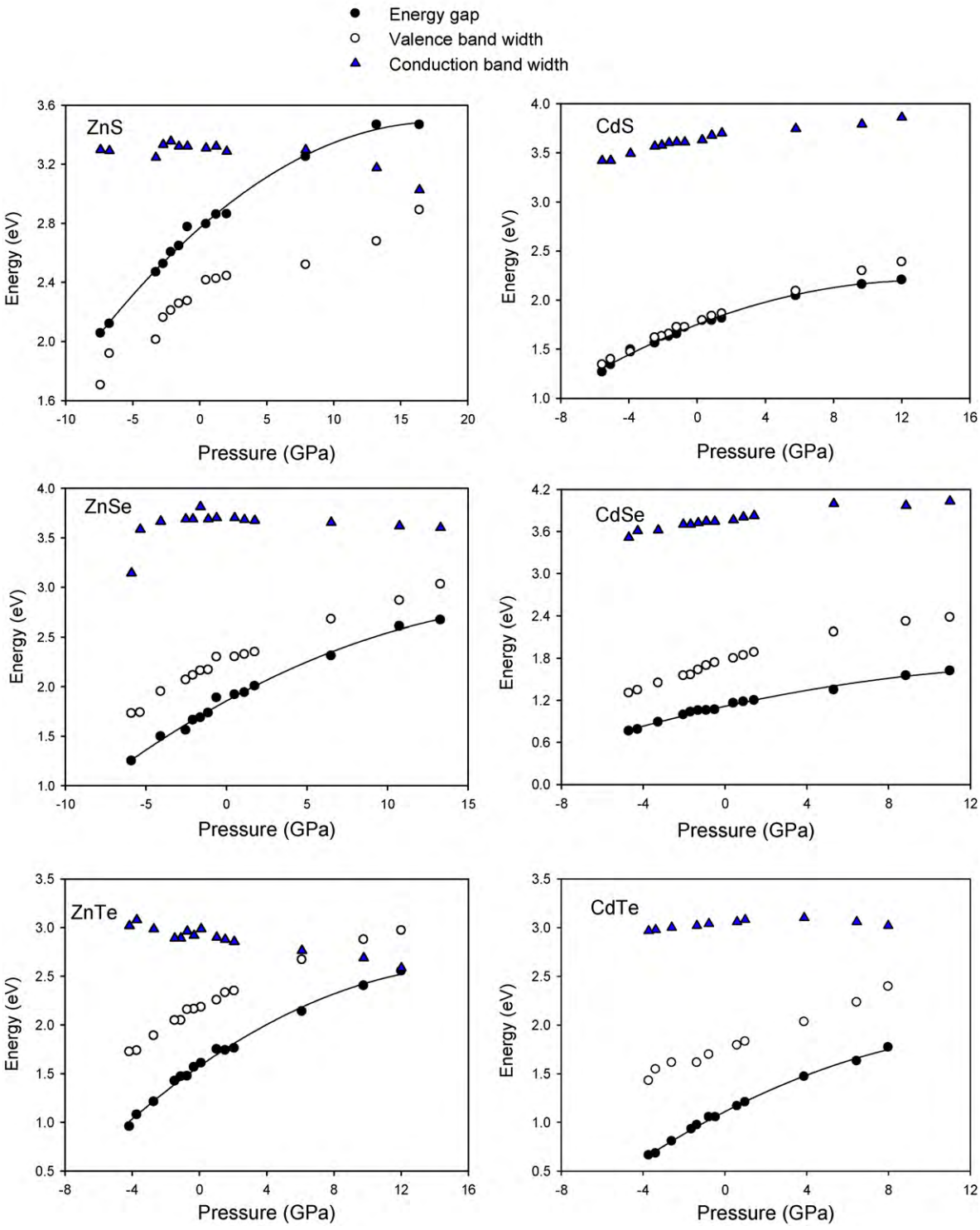

Fig. 4. The calculated energy band gap, valence and conduction bands width as a function of pressure within GGA_EV.

top valence band, and reduces the linear pressure coefficient. The second order pressure coefficients of these compounds are small.

3.3. Optical properties

The optical properties of matter can be described by means of the transverse dielectric function $\varepsilon(\omega)$. There are two contributions to $\varepsilon(\omega)$, namely, intraband and interband transitions. The contribution from intraband transitions is important only for metals. The interband transitions can further be split into direct and indirect transitions. Here the indirect interband transitions which involve scattering of phonons and are expected to give only a small contribution to $\varepsilon(\omega)$ [77] are neglected. To calculate the direct interband contribution to the imaginary part of the dielectric function, $\varepsilon_2(\omega)$, one must sum up all possible transitions from the occupied to the unoccupied states. Taking the appropriate transition matrix ele-

Table 5
The first and second order pressure coefficients of energy band gap within GGA_EV.

Compounds	E_g^0 (eV)	$\alpha \times 10^{-2}$eV (GPa)$^{-1}$			$\beta \times 10^{-3}$eV (GPa)$^{-2}$		
		This work	Expt.	Other work	This work	Expt.	Other work
ZnS	3.26	5.47	6.35[a]	6.22[a]	−2.19	−1.31[a]	−1.14[a]
			5.7				−1.826[b]
ZnSe	2.34	6.26	7.0[a]	5.40[b]	−2.0	–	−1.516[b]
ZnTe	1.80	10.71	10.3[c]	7.03[b]	−3.53	−2.4[c]	−1.602[b]
CdS	1.94	5.02	4.5[d]	2.8[e]	−1.24	–	–
CdSe	1.40	5.53	5.0[d]	3.35[e]	−1.74	–	–
CdTe	1.30	9.47	8.0[d]	8.39[e]	−3.69	–	–

[a] Ref. [75].
[b] Ref. [37].
[c] Ref. [76].
[d] Ref. [29].
[e] Ref. [38].

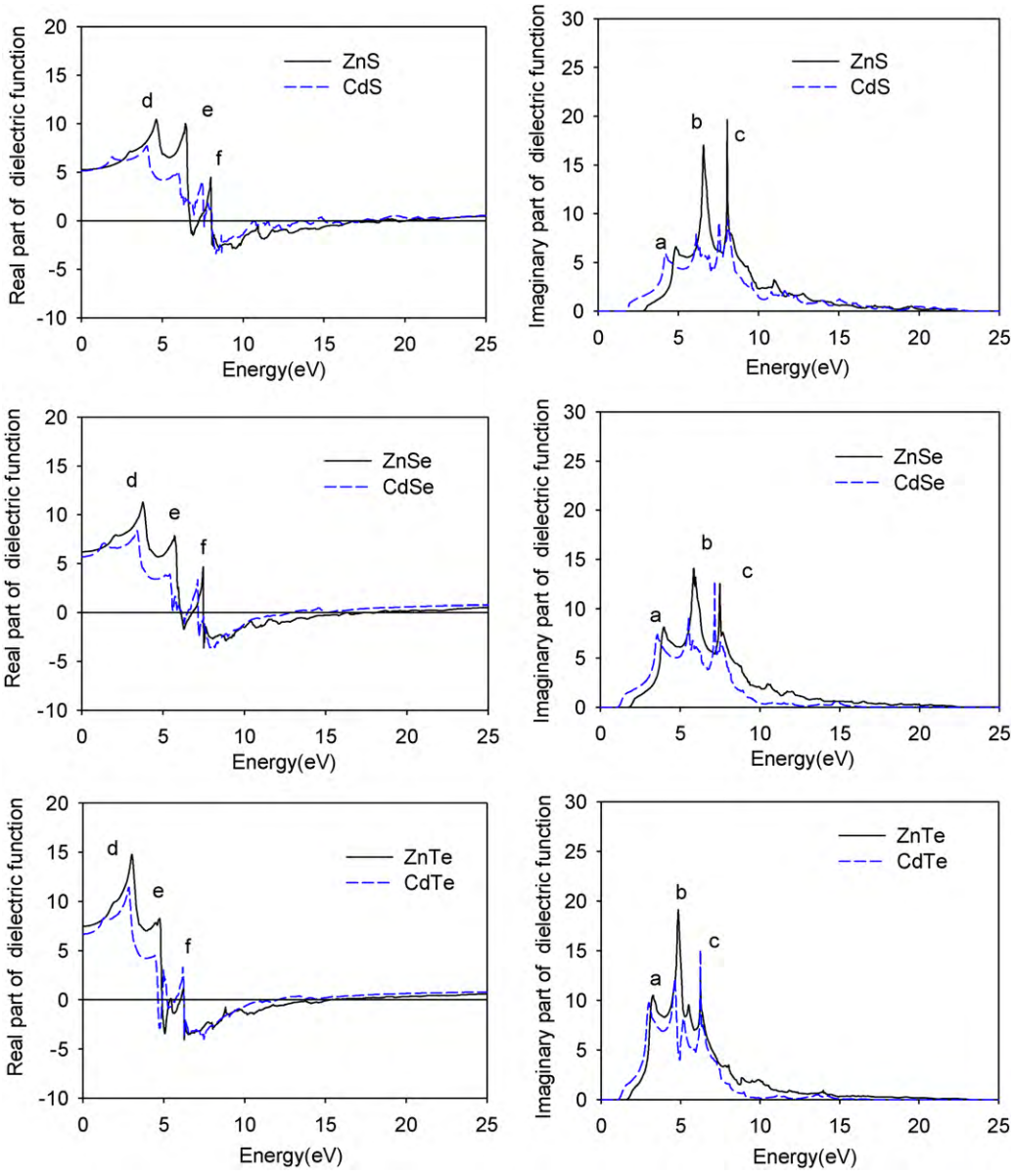

Fig. 5. The calculated real and imaginary parts of dielectric function of ZnX and CdX compounds within GGA_EV.

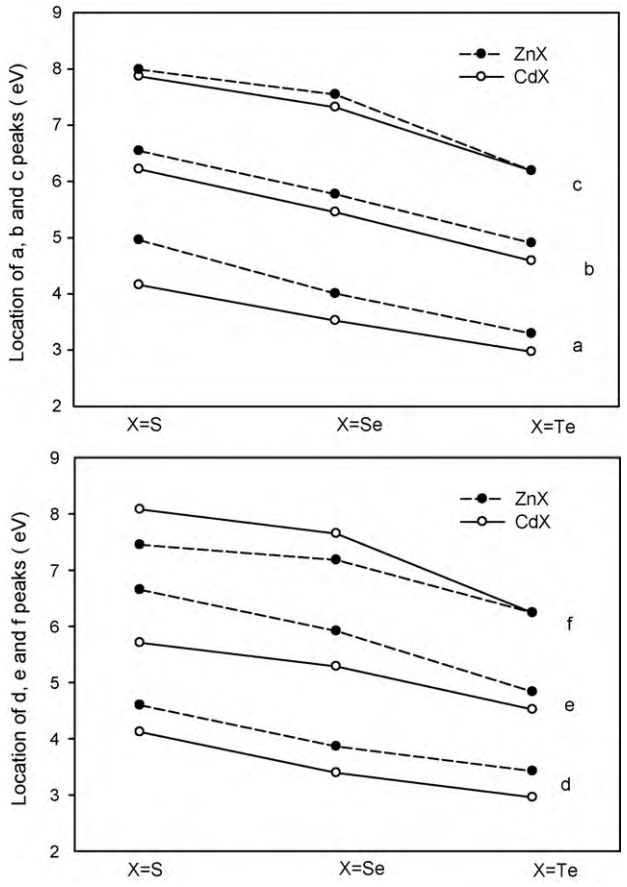

Fig. 6. The locations of imaginary and real parts of dielectric function peaks (labeled a–f in Fig. 5) within GGA_EV.

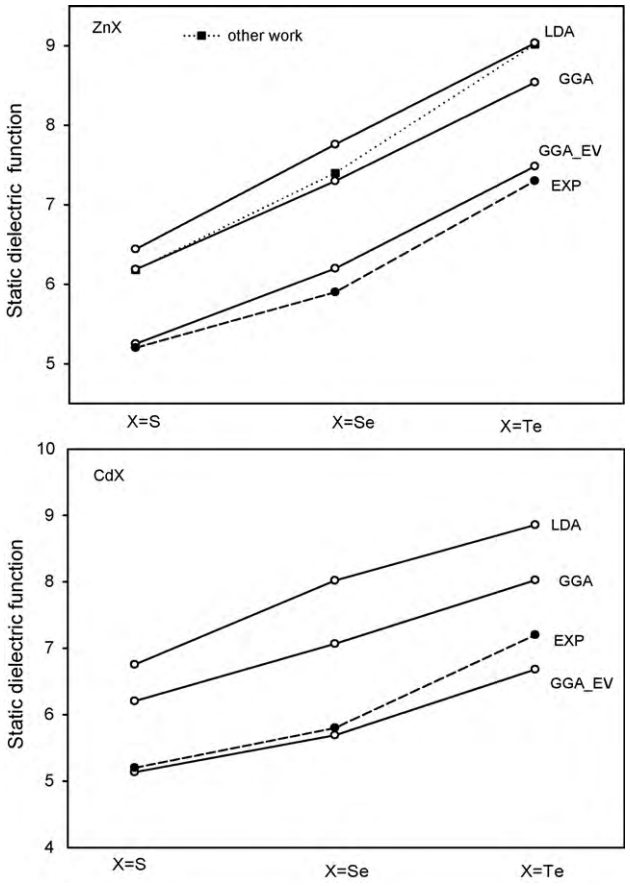

Fig. 7. The calculated static dielectric function of ZnX and CdX compounds within LDA, GGA, GGA_EV and experimental values and other work. The black squares represent the other works for ZnX compounds.

ments into account, the imaginary part of the frequency dependent dielectric function $\varepsilon_2(\omega)$ is given by:

$$\varepsilon_2(\omega) = \frac{Ve^2}{2\pi\hbar m^2\omega^2}\int d^3k \sum_{nn'} \left|\left\langle \vec{K}_n \right| \vec{p} \left| \vec{K}_{n'} \right\rangle\right|^2 f(\vec{K}_n)[1 - f(\vec{K}_{n'})]\delta(E_{\vec{K}_n} - E_{\vec{K}_{n'}} - \hbar\omega) \tag{1}$$

where $\hbar\omega$ is the energy of the incident photon, p is the momentum operator $(\hbar/i)(\partial/\partial x)$, $|kn\rangle$, is the eigenfunction with eigenvalue E_{kn} and $f(\vec{kn})$ is the Fermi distribution function. The evaluation of the matrix elements of the momentum operator in Eq. (1) is performed over the muffin-tin and the interstitial regions separately. A detailed description of the calculation of these matrix elements is given by Ambrosch-Draxl et al. [78]. The real part of the dielectric function $\varepsilon_1(\omega)$ follows from the Kramers–Kronig relation:

$$\varepsilon_1(\omega) = 1 + \frac{2}{\pi}\int_0^\infty \frac{\varepsilon_2(\omega')\omega' d\omega'}{\omega'^2 - \omega^2} \tag{2}$$

The optical constants such as the reflectivity $R(\omega)$, the absorption coefficient $I(\omega)$, and the electron energy loss function $L(\omega)$ can be calculated, using the dielectric function, through the following relations:

$$R(\omega) = \left|\frac{\sqrt{\varepsilon(\omega)} - 1}{\sqrt{\varepsilon(\omega)} + 1}\right|^2 \tag{3}$$

$$I(\omega) = 2\omega\left(\frac{[\varepsilon_1(\omega)^2 + \varepsilon_2(\omega)^2] - \varepsilon_1(\omega)}{2}\right)^{1/2} \tag{4}$$

$$L(\omega) = \frac{\varepsilon_2(\omega)}{\varepsilon_1(\omega)^2 + \varepsilon_2(\omega)^2} \tag{5}$$

In order to calculate $\varepsilon_1(\omega)$, one needs to have a good representation of $\varepsilon_2(\omega)$ up to high energies. The author has calculated $\varepsilon_2(\omega)$ up to 95 eV above the Fermi level and has used this value as the truncation energy in Eq. (2). This energy range was chosen so as to produce convergence in the Kramers–Kronig transformation.

To investigate the optical properties of ZnX and CdX compounds, the author has considered only the cubic phase of these compounds. Since these compounds have cubic symmetry, the author needs to calculate only one dielectric tensor component to completely characterize the linear optical properties. The calculated results within LDA are performed using the calculated equilibrium lattice constant according to LDA. The author has calculated energy dependent real and imaginary parts of the dielectric function for ZnX and CdX compounds within LDA, GGA and GGA_EV, using the equilibrium lattice constant according to GGA. Due to a close similarity between the resulting curves, the dielectric functions are shown in Fig. 5 for GGA_EV only. The calculated $\varepsilon_2(\omega)$ has three major peaks, labeled a, b and c in Fig. 5. The locations of these peaks are shown in Fig. 6. Although there is a reasonable agreement between the $\varepsilon_2(\omega)$ curves within LDA, GGA (not shown in Fig. 5) and GGA_EV, the locations of the peaks do not coincide. This is due to the fact that band structures of these compounds are similar with different band splitting. The peaks of the imaginary part of the dielectric function within GGA and GGA_EV related to LDA shift toward higher energies. This shift for GGA is smaller than the corresponding value within GGA_EV. This trend may be directly inferred from the band structure and electron density of states results. The LDA and GGA band struc-

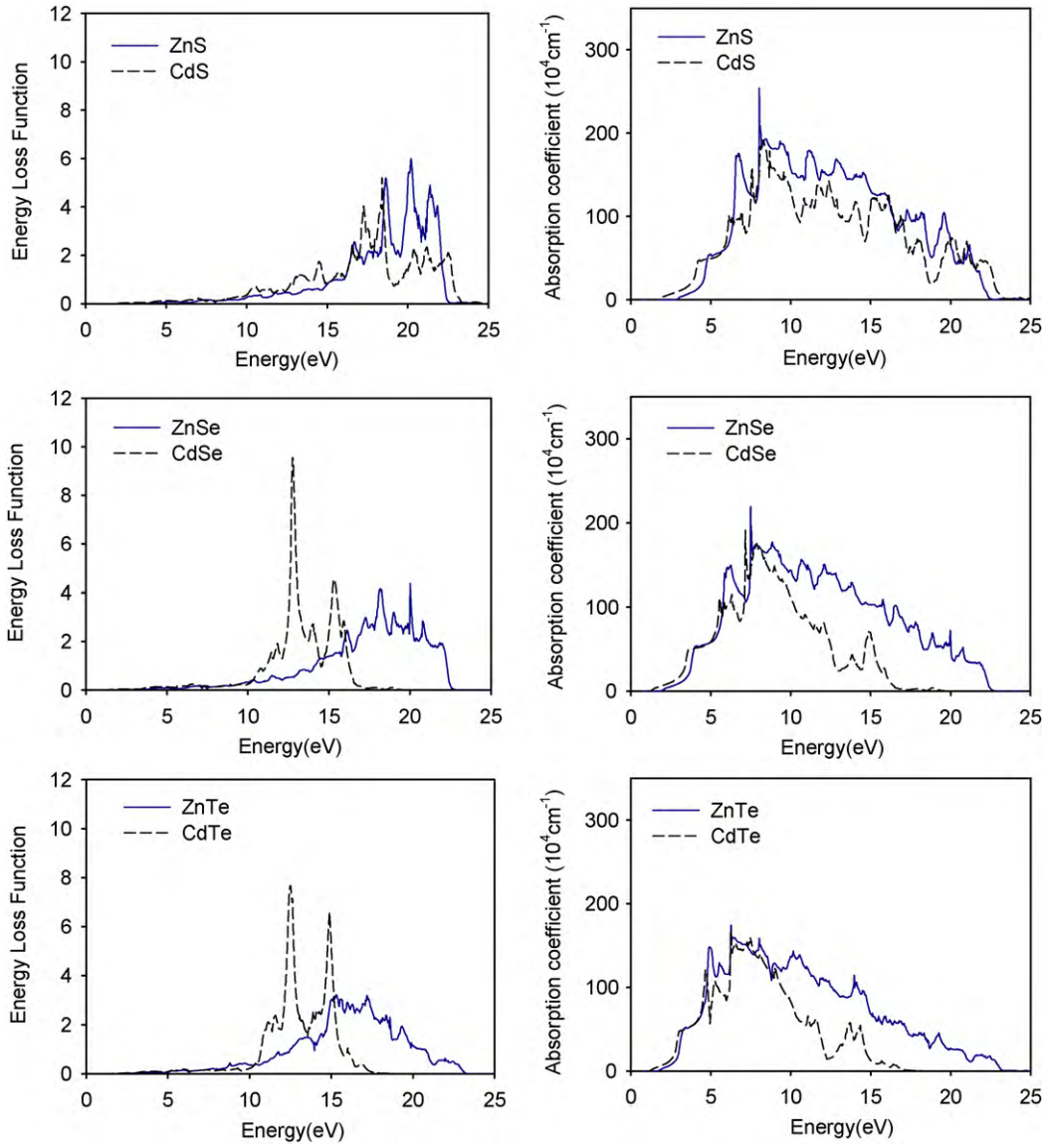

Fig. 8. The calculated energy loss function and the absorption coefficient of ZnX and CdX compounds within GGA_EV using the equilibrium lattice constant according to GGA.

ture calculations underestimate the gap values and therefore have lower peak positions. The calculated energy dependent imaginary parts of the dielectric function of ZnX and CdX compounds show that all structures in $\varepsilon_2(\omega)$ shift toward the lower energies with reduced peak heights when Zn is replaced by Cd. This is due to the reduction in the energy band gaps. The most important contribution to the peak in all compounds is due to the transition from the maximum of the valence band to the minimum of the conduction band. The onset of the absorption edge in $\varepsilon_2(\omega)$ corresponds to a direct transition from the highest valence band at the Γ point to the lowest conduction band at Γ point. Peak b arises principally from a transition along $\Gamma L W$ direction in the BZ. The c peak is due to the transition from lower bands to higher bands. Freeouf [35] and Ghahramani et al. [79] measured and calculated the $\varepsilon_2(\omega)$ for ZnS, ZnSe and ZnTe compounds. The main features of Freeouf and Ghahramani et al. results are: three peaks for ZnS and ZnSe around 6 eV and 6.5 eV (the strongest), around 7 eV and 6.5 eV with relative intensities of about 0.91 and 0.60, around 6 eV and 8.5 eV with relative intensities of about 0.40 and 0.37. There are five peaks for ZnTe around 5 eV (the strongest), around 4.5 eV with a relative intensity of about 0.77, around 3.75 eV with relative intensity of about 0.71, around 7 eV with a relative intensity of about 0.50 and around 7.45 eV with relative intensity of about 0.42. Comparing the calculated imaginary part of the dielectric function of ZnS, ZnSe and ZnTe compounds with the Freeouf and Ghahramani results, the author has concluded that the location of peaks within GGA_EV related to LDA and GGA are in better agreement with experiment. The calculated imaginary parts of the dielectric function of CdS, CdSe and CdTe show that the calculated results within GGA_EV are in better agreement with available experimental results [14,38,40]. This is to be expected, since GGA_EV improves the band structure calculation, which has considerable effect on optical properties. The p states of X atom and the d states of Zn and Cd play a major role in these optical transitions as initial and final states.

The calculated real parts of the dielectric function of ZnX and CdX compounds, $\varepsilon_1(\omega)$, within GGA_EV have three peaks (around 3–4.5 eV, 3.5–6.5 eV and 6.5–8 eV) labeled d, e and f: a rather steep decrease between 5 eV and 6 eV, where $\varepsilon_1(\omega)$ starts to become negative and a minimum with slow increase toward zero. Cardona and Harbeke [80] and Freeouf [35] measured the real part of the dielectric function of ZnSe and ZnS compounds. A comparison of the calculated results with Cardona and Freeouf and other avail-

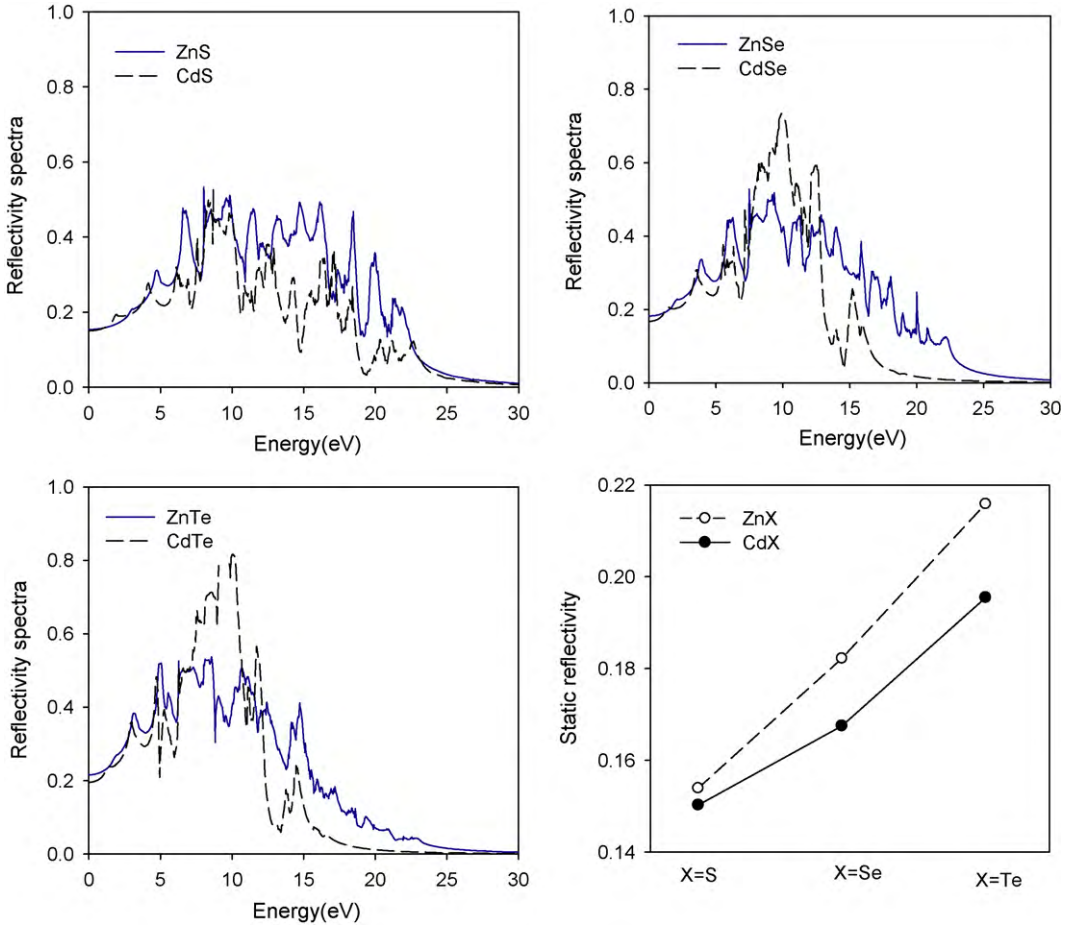

Fig. 9. The calculated reflectivity spectra and the static reflectivity spectra of ZnX and CdX compounds within GGA_EV using the equilibrium lattice constant according to GGA.

able experimental results shows that the calculated real part of the dielectric function of ZnX and CdX compounds within GGA-EV related to LDA and GGA is in better agreement with experiment. The real parts of the dielectric function of ZnX and CdX compounds decrease when Zn is replaced by Cd. The locations of the three peaks of $\varepsilon_1(\omega)$ are also shown in Fig. 6. These peaks shift toward lower energies with reduced peak height when Zn is replaced by Cd. The location of these peaks shifts toward higher energies when Te is replaced by Se and Se by S. The static dielectric function, ε^0, is a very important physical quantity for semiconductors. The calculated ε^0 values within LDA, GGA and GGA_EV, experimental values [6,81] and other available works [37] for all compounds are shown in Fig. 7. The calculated ε^0 of these compounds within GGA_EV is in better agreement with experiment compared to other available theoretical work which is based on LDA. LDA and GGA overestimate the static dielectric function ε^0 as a consequence of the energy band gap underestimation. For the same X atom the static dielectric function of ZnX is larger than CdX and increases as the atomic number of X atom increases. This trend in the static dielectric function is in agreement with experimental data.

The energy loss function ($L(\omega)$) is an important factor describing the energy loss of fast electrons traversing in the material. The author has calculated $L(\omega)$ and the absorption coefficient ($I(\omega)$) of ZnX and CdX compounds within LDA, GGA and GGA_EV. The calculated $L(\omega)$ and $I(\omega)$ within GGA_EV are shown in Fig. 8. The energy loss spectra of ZnX and CdX do not show significant value in energies smaller than about 10 eV. The reason for this is that $\varepsilon_2(\omega)$ is large at these energy values. But in an energy range of 10–0 eV there are some large peaks in the energy loss spectra. At such high energies $\varepsilon_2(\omega)$ are small and the amplitude of the energy loss function becomes large. The energy loss function shifts toward higher energies when Te is replaced by Se and Se by S. For the same X atom the energy loss function shifts toward higher energies when Zn is replaced by Cd. The calculated energy dependent absorption coefficient has some peaks in the energy range of 5–0 eV. The partial electron density of states of ZnX and CdX compounds show that the Zn d and Cd d electrons increase the absorption coefficient around 5–0 eV (5–5 eV for ZnS) and 5–5 eV for ZnX and CdX compounds respectively and reduce it else where.

The author has calculated the reflectivity spectra of these compounds within GGA, LDA and GGA_EV. The reflectivity spectra within GGA_EV are shown in Fig. 9. In all compounds the reflectivity spectra are small in the low energy region, the reflectivity spectra of ZnX and CdX compounds within LDA, GGA (not shown in Fig. 9) and GGA_EV are similar. The location of the reflectivity peaks within GGA_EV related to LDA and GGA shift toward the higher energy. The reflectivity starts at around 20% for all compounds and reaches the maximum value of about 55% for ZnS, ZnSe, ZnTe and CdS compounds and about 80% for CdSe and CdTe compounds. This shift is due to the shifting of d electron density of states toward higher energies. Freeouf [35] and Cardona and Harbeke [80] measured the reflectivity spectra for ZnS and ZnSe compounds. Comparing the calculated results with Freeouf and Cardona shows that the reflectivity spectra of these compounds (within GGA_EV) are in better agreement with experiment. The author has calculated the static reflectivity R^0 within GGA_EV. The calculated results are also shown in Fig. 9. To my knowledge no experimental or theoretical data for the static reflectivity of these compounds are available to be com-

pared with. The calculated results show that the static reflectivity of ZnX is larger than CdX and increases as the atomic number of X atom increases.

3.4. Effect of pressure on optical properties

At this part I am interested to study the pressure dependence of the optical properties of these compounds. To investigate the effect of pressure on optical properties of ZnX and CdX compounds, the author has calculated the real and imaginary parts of the dielectric function within GGA_EV at different pressures. The pressure is calculated within GGA. Due to the close similarity between the behavior of the real and imaginary parts of the dielectric function of these compounds under pressure, the real and imaginary parts of the dielectric function at three different pressures are shown only for ZnS compound in Fig. 10. Under pressure, the positions of all critical points shift toward higher energies. The reason lies in the enhancement of the direct band gaps under pressure. Although peak positions shift under pressure, these peaks still have the same shape as that have at zero pressure except that the real and imaginary parts of dielectric function magnitude increase. Khenata et al. [37] studied the effect of pressure on the static dielectric function of ZnX compounds using LDA. They conclude that the increase of the dielectric functions with pressure is linear. The author has calculated the static dielectric function and the static reflectivity of ZnX and CdX compounds within GGA_EV at different pressures. The calculated results are shown in Fig. 11. The results show that the variation of the static dielectric function and the reflectivity with pressure is not linear. The calculated ε^0 and R^0 are fitted to second order polynomials:

$$\varepsilon^0(p) = \varepsilon^0(0) + ap + bp^2$$
$$R^0(p) = R^0(0) + cp + dp^2$$

where p(GPa) is the pressure, $\varepsilon^0(0)$ and $R^0(0)$ are the static dielectric function and the static reflectivity at zero pressure, $a(c)$ and $b(d)$ are the first and second order pressure coefficients of the static dielectric function (the static reflectivity) which are given in Table 6. To

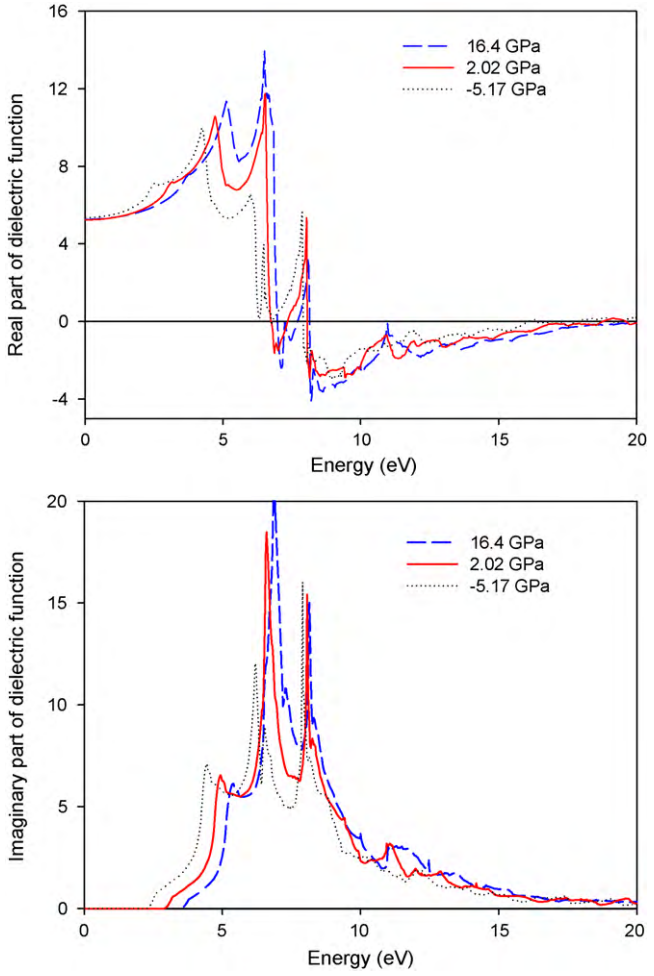

Fig. 10. The real and imaginary parts of the dielectric function of ZnS compound within GGA_EV at three different pressures.

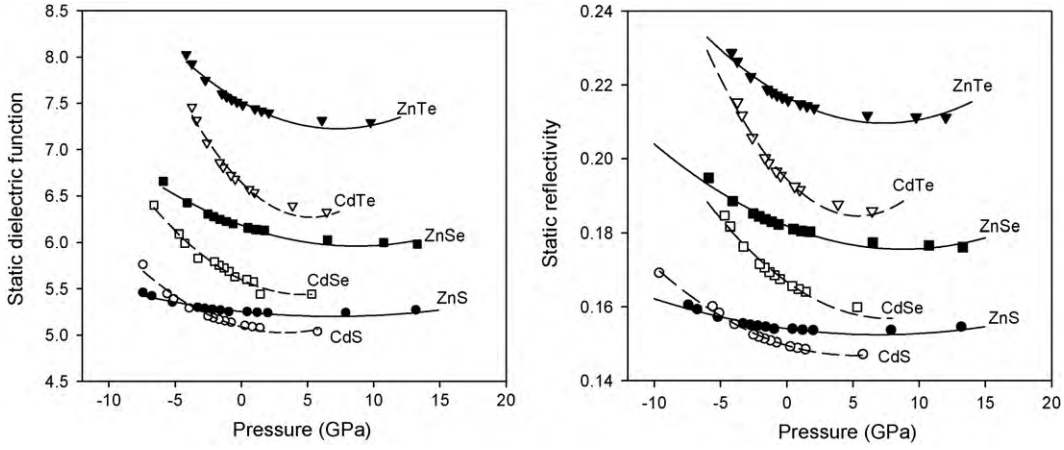

Fig. 11. The calculated static dielectric function and the static reflectivity within GGA_EV depending on pressure.

Table 6
The first and second order pressure coefficients of static dielectric function and static reflectivity within GGA_EV.

Compounds	$\varepsilon^0(0)$	$a \times 10^{-2}$	$b \times 10^{-3}$	$R^0(0)$	$c \times 10^{-4}$	$b \times 10^{-5}$
ZnS	5.24	−1.51	1.34	0.15	−4.72	4.19
ZnSe	6.18	−5.09	2.93	0.18	−14.14	8.03
ZnTe	7.52	−8.05	5.53	0.21	−19.22	13.11
CdS	5.08	−3.80	5.84	0.15	−10.70	10.69
CdSe	5.60	−6.88	7.33	0.16	−24.84	26.20
CdTe	6.63	−14.40	16.15	0.19	−37.37	40.73

the best of my knowledge no experimental or theoretical data for the static dielectric function (of CdX compounds) and static reflectivity (of ZnX and CdX compounds) as a function of pressure are available to be compared with. The magnitude of the first order pressure coefficients (a and c) of CdX are larger than those of ZnX and increase with increasing X atomic number.

4. Conclusions

The author has studied the structural, electronic and optical properties of ZnX and CdX compounds within LDA, GGA and GGA_EV. The calculated energy band gap of these compounds within LDA, GGA and GGA_EV shows that the GGA_EV yields better values for energy band gaps, with respect to experimental values. The calculated optical properties of ZnX and CdX compounds show that the real and imaginary parts of the dielectric function and the reflectivity spectra within GGA_EV are in better agreement with experiment. Furthermore, the author has calculated the energy band gap, static dielectric function and static reflectivity at different pressures and fitted the results to a second order polynomial. The valence band width increases with pressure that enhances the covalent character and hence decreases the ionicity of these compounds. The author has studied the behavior of the energy band gap and the optical properties of ZnX and CdX compounds under pressure. The author has found that under pressure, the structures in the real and imaginary parts of the dielectric function shift toward higher energies.

References

[1] M. Durandurdu, J. Phys. Chem. Solids 70 (2009) 645.
[2] K. Wright, J.D. Gale, Phys. Rev. B 70 (2004) 035211.
[3] S. Cui, H. Hu, W. Feng, X. Chen, Z. Feng, J. Alloys Compd. 472 (2009) 294.
[4] Su.-H. Wei, S.B. Zhang, Phys. Rev. B 62 (2000) 6944.
[5] X. Cao, C. Zhao, X. Lan, D. Yao, W. Shen, J. Alloys Compd. 474 (2009) 61.
[6] S.M. Hosseini, Physica B 403 (2008) 1907.
[7] C. Bealing, R. Martoňák, C. Molteni, Solid State Sci. 12 (2010) 157.
[8] Y. Al-Douri, Mater. Chem. Phys. 78 (2003) 625.
[9] H. Sowa, Solid State Sci. 7 (2005) 73.
[10] C. He, C. Gao, Y. Ma, B. Lin, M. Li, X. Huang, A. Hao, C. Yu, D. Zhang, H. Liu, G. Zou, J. Phys. Chem. Solids 69 (2008) 2227.
[11] H. Sowa, Solid State Sci. 7 (2005) 1384.
[12] J.Z. Hu, Solid State Commun. 63 (1987) 471.
[13] T. Tsuchiya, S. Ozaki, S. Adachi, J. Phys. Condens. Matter 15 (2003) 3717.
[14] M.-Z. Huang, W.Y. Ching, Phys. Rev. B 47 (1993) 9449.
[15] A. Pan, R. Liu, F. Wang, S. Xie, B. Zou, M. Zacharias, Z.L. Wang, J. Phys. Chem. B 110 (2006) 22313.
[16] C. Baban, G.I. Rusu, P. Prepelita, J. Optoelectron. Adv. Mater. 7 (2005) 817.
[17] Q. Zhai, J. Li, J.S. Lewis, K.A. Waldrip, K. Jones, P.H. Holloway, M. Davidson, N. Evans, Thin Solid Films 414 (2002) 105.
[18] E. Erbarut, Solid State Commun. 127 (2003) 515.
[19] S. Tomimoto, S. Nozawa, Y. Terai, S. Kuroda, K. Takita, Y. Masumoto, Phys. Rev. B 81 (2010) 125313.
[20] E.R. Shaaban, N. Afify, A. El-Taher, J. Alloys Compd. 482 (2009) 400.
[21] B.R. Salles, K. Kunc, M. Eddrief, V.H. Etgens, F. Finocchi, F. Vidal, Phys. Rev. B 79 (2009) 155312.
[22] S. Sapra, N. Shanthi, D.D. Sarma, Arxiv: Condens. Matter 4 (2003) 0308048.
[23] R.R. Reddy, K. Rama Gopal, K. Narasimhulu, L. Siva Sankara Reddy, K. Raghavendra Kumar, G. Balakrishnaiah, M. Ravi Kumar, J. Alloys Compd. 473 (2009) 28.
[24] B.D. Rajput, D.A. Browne, Phys. Rev. B 53 (1996) 9052.
[25] F. Benkabou, H. Aourag, M. Cartier, Mater. Chem. Phys. 66 (2000) 10.
[26] M. Kitamura, S. Muramatsu, W.A. Harrison, Phys. Rev. B 46 (1992) 1351.
[27] I. Sarkar, M.K. Sanyal, S. Takeyama, S. Kar, H. Hirayama, H. Mino, F. Komori, S. Biswas, Phys. Rev. B 79 (2009) 054410.
[28] Y. Yamada, Y. Masumoto, T. Taguchi, K. Takemura, Phys. Rev. B 44 (1991) 1801.
[29] P.Y. Yu, M. Cardona, Fundamentals of Semiconductors Physics and Materials Properties, Springer-Verlag, Berlin, 2001 (Chapter 7).
[30] J.R. Chelikowsky, Phys. Rev. B 35 (1987) 1174.
[31] Y. Yu, J. Zhou, H. Han, C. Zhang, T. Cai, C. Song, T. Gao, J. Alloys Compd. 471 (2009) 492.
[32] A.H. Reshak, S. Auluck, Physica B 395 (2007) 143.
[33] S.Zh. Karazhanov, P. Ravindran, A. Kjekshus, H. Fjellvåg, B.G. Svensson, Phys. Rev. B 75 (2007) 155104.
[34] C.Y. Bang, M.S. Lee, T.J. Kim, Y.D. Kim, D.E. Aspnes, Y.M. Yu, B. Sung, Y.D. Choi, I. Korean, J. Korean Phys. Soc. 39 (2001) 462.
[35] J.L. Freeouf, Phys. Rev. B 7 (1973) 3810.
[36] D. Ronnow, M. Cardona, L.F. Lastras-Martinez, Phys. Rev. B 59 (1999) 5581.
[37] R. Khenata, A. Bouhemadou, M. Sahnoun, A.H. Reshak, H. Baltache, M. Rabah, Comput. Mater. Sci. 38 (2006) 29.
[38] E. Deligoz, K. Colakoglu, Y. Ciftci, Physica B 373 (2006) 124.
[39] D. Kirin, I. Lukačević, Phys. Rev. B 75 (2007) 172103.
[40] A.E. Merad, M.B. Kanoun, G. Merad, J. Cibert, H. Aourag, Mater. Chem. Phys. 92 (2005) 333.
[41] J.P. Perdew, A. Zunger, Phys. Rev. B 23 (1981) 5048.
[42] J.P. Perdew, K. Burke, M. Ernzerhof, Phys. Rev. Lett. 77 (1996) 3865.
[43] E. Engel, S.H. Vosko, Phys. Rev. B 50 (1994) 10498.
[44] P. Blaha, K. Schwarz, J. Luitz, WIEN97, A full potential linearized augmented plane wave package for calculating crystal properties, Karlheinz Schwarz, Techn. Universitat Wien, Austria, 1999, ISBN 3-9501031r-r0-4.
[45] O. Zakharov, A. Rubio, X. Blase, M.L. Cohen, S.G. Louie, Phys. Rev. B 50 (1994) 10780.
[46] N. Lakshmi, N.M. Rao, R. Venugopal, D.R. Reddy, B.K. Reddy, Mater. Chem. Phys. 82 (2003) 764.
[47] H. Schulz, K.H. Thiemann, Solid State Commun. 32 (1979) 783.
[48] F.D. Murnaghan, Proc. Natl. Acad. Sci. U.S.A. 30 (1944) 244.
[49] S. Desgreniers, L. Beaulieu, I. Lepage, Phys. Rev. B 61 (2000) 8726.
[50] L. Ley, A. Pollak, F.R. McFeely, S. Kowalczyk, D.A. Shirley, Phys. Rev. B 9 (1974) 600.
[51] A. Qteish, R. Said, N. Meskini, A. Nazzal, Phys. Rev. B 52 (1995) 1830.
[52] F. El Haj Hassan, S.J. Hashemifar, H. Akbarzadeh, Phys. Rev. B 73 (2006) 195202.
[53] B.K. Agrawal, P.S. Yadav, S. Agrawal, Phys. Rev. B 50 (1994) 14881.
[54] So.J. Yun, G. Lee, J.S. Kim, S.K. Shin, Y.-G. Yoon, Solid State Commun. 137 (2006) 332.
[55] O. Madelung (Ed.), Numerical Data and Functional Relationship in Science and Technology, Landolt_Börnstein, New Series Group III, vol. 17, Springer-Verlag, Berlin, 1982.
[56] M.L. Cohen, Phys. Rev. B 32 (1985) 7988.
[57] Y. Al-Douri, H. Abid, A. Zaoui, H. Aourag, Physica B 301 (2001) 295.
[58] Y. Al-Douri, H. Abid, H. Aourag, Physica B 322 (2002) 179.
[59] Y. Al-Douri, H. Abid, H. Aourag, Physica B 305 (2001) 186.
[60] P. Dufek, P. Blaha, K. Schwarz, Phys. Rev. B 50 (1994) 7279.
[61] A. Qteish, M. Parrinello, Phys. Rev. B 61 (2000) 6521.
[62] X.-R. Chen, X.-F. Li, L.-C. Cai, J. Zhu, Solid State Commun. 139 (2006) 246.
[63] A. Qteish, A. Muñoz, J. Phys. Condens. Matter 12 (2000) 1705.
[64] K. Kusaba, T. Kikegawa, J. Phys. Chem. Solids 63 (2002) 651.
[65] A. San-Mignel, A. Polian, J.P. Itie, A. Marbeuf, R. Triboulet, High Press. Res. 10 (1992) 412.
[66] G.-D. Lee, J. Ihm, Phys. Rev. B 53 (1996) R7622.
[67] J.D. Kennedy, W.B. Benedick, J. Phys. Chem. Solids 27 (1966) 125.
[68] M.D. Knudson, Y.M. Gupta, A.B. Kunz, Phys. Rev. B 59 (1999) 11704.
[69] R. Gangadharan, V. Jayalakshmi, J. Kalaiselvi, S. Mohan, R. Murugan, B. Palanivel, J. Alloys Compd. 359 (2003) 22.
[70] M.I. McMahon, R.J. Nelmes, N.G. Wright, D.R. Allan, Phys. Rev. B 48 (1993) 16246.
[71] V.I. Smelyansky, J.S. Tse, Phys. Rev. B 52 (1995) 4658.
[72] V.V. Shchennikov, S.V. Ovsyannikov, Phys. Status Solidi (b) 244 (2007) 437.
[73] A. Mujica, A. Rubio, A. Muñoz, R.J. Needs, Rev. Mod. Phys. 75 (2003) 863.
[74] M. Catti, Phys. Rev. B 65 (2002) 224115.
[75] K. Reimann, M. Haselhoff, St. Rubenacke, M. Steube, Phys. Status Solidi (b) 198 (1996) 71.
[76] B. Gil, D.J. Dunstan, Semicond. Sci. Technol. 6 (1991) 428.
[77] N.V. Smith, Phys. Rev. B 3 (1971) 1862.
[78] C. Ambrosch-Draxl, J.A. Majewski, P. Vogl, G. Leising, Phys. Rev. B 51 (1995) 9668.
[79] Ed. Ghahramani, D.J. Moss, J.E. Sipe, Phys. Rev. B 43 (1991) 9700.
[80] M. Cardona, G. Harbeke, Phys. Rev. 137 (1965) A1467.
[81] C.S. Wang, B.M. Klein, Phys. Rev. B 24 (1981) 3417.